

OPEN

Interface treatment using amorphous-carbon and its applications

Myung Sik Choi^{1,5}, Han Gil Na^{1,5}, Jae Hoon Bang¹, Sun-Woo Choi², Sang Sub Kim³,
Kyu Hyoung Lee⁴, Hyoun Woo Kim^{1*} & Changhyun Jin^{4*}

Breakthrough process technologies have been introduced that can increase the chemical sensitivity of an interface at which reactions occur without significantly altering the physico-chemical properties of the material. Such an interfacial treatment method is based on amorphous-carbon as a base so that fluids can be deposited, and the desired thickness and quality of the deposition can be ensured irrespective of the interface state of the material. In addition, side effects such as diffusion and decreasing strength at the interface can be avoided. This is simpler than existing vacuum-based deposition technology and it has an unmatched industrial advantage in terms of economics, speed, accuracy, reliability, accessibility, and convenience. In particular, this amorphous-carbon interface treatment technology has been demonstrated to improve gas-sensing characteristics of NO₂ at room temperature.

Techniques such as electroplating¹, electroless plating², anodisation³, chemical treatment⁴, plasma surface treatment⁵, and dry coating⁶, in which one or more thin layers are overlaid on a material, protect the surface of the material⁷, increase its strength⁸, and add functionality⁹. And most of these technologies are limited to bulk materials, rather than nanomaterials, such as automotive-, machine-, tool-, and mold-materials^{10–13}, based on progress in science/engineering. Also, as the manufacture of thin films¹⁴ and core-shell structures¹⁵ by vacuum deposition¹⁶ and vacuum coating¹⁷ is gaining momentum, particularly for home appliances, electronic components, optical components, and biomaterials^{18–20}, sub-factors such as clean technology, evaporation source selectivity, product-specific process technologies, and functional deposition materials, became one of the main technologies. However, in order to realise the manufacture of complete thin films/coatings such as natural simulation^{21,22}, engineered structure implementation using hybrid processes^{23,24}, high-speed deposition²⁵, and cost-saving technology²⁶, many problems have to be overcome, as follows.

- (1) The state of the surface of a material may significantly influence the adhesion of the thin film/coating and the characteristics and life of the product; hence, an extra process must be performed to remove the impurities and the oxide film²⁷.
- (2) Although the process itself is simple, the evaporation technique is unidirectional. Therefore, step coverage cannot be avoided²⁸.
- (3) Deposition via metal-organic chemical vapour deposition (MOCVD) has the disadvantage that growth rate and impurity doping are possible only with substrate temperature and gas flow rate, but using hazardous materials and high equipment/source cost²⁹.
- (4) Deposition via atomic layer deposition (ALD) has the advantages of thin film deposition and low impurity content on an atomic level, but the deposition rate is limited by the ALD mechanism³⁰.
- (5) Sputtering can be used to control certain aspects of thin films of difficult materials, such as high melting points, but it requires large amounts of gas for ionisation and its efficiency is poor³¹.

¹Division of Materials Science and Engineering, Hanyang University, Seoul, 04763, Republic of Korea. ²Department of Materials Science and Engineering, Kangwon National University, Samcheok, 25913, Republic of Korea. ³Department of Materials Science and Engineering, Inha University, Incheon, 402-751, Republic of Korea. ⁴Department of Materials Science and Engineering, Yonsei University, Seoul, 03722, Republic of Korea. ⁵These authors contributed equally: Myung Sik Choi and Han Gil Na. *email: hyounwoo@hanyang.ac.kr; chjin0910@gmail.com

As described above, an advantage in one process can be a disadvantage in the other; hence, based on many considerations, the best process can be determined depending on which factors one focuses on. Processes or deposition/coating techniques with many advantages at the same time have not yet been introduced or tested. In addition, when a heterogeneous material is deposited on an existing product or substrate to form a new double layer, the properties of the individual materials may be lost owing to interdiffusion³² between the two materials. Even if the interdiffusion is controlled, because the arrangement of irregular atoms at the bonding interface cannot be avoided, the strength of the irregular atoms must be lower than that of the matrix. As such, the bonding interface of the heterogeneous materials cannot but react sensitively, unlike the inner parts of the material. If so, is there no means of enhancing the properties of existing materials while increasing the adsorption strength during adsorption to other materials? If one considers several prerequisites to take only the selfish advantage, the following conditions must be met. First, in order to increase the adsorption strength regardless of the state of the other interfaces of all products, the deposition material must have characteristics that enable it to cover the substrate like a fluid. Second, in order to increase the characteristics of the coated material, it is necessary to reduce the characteristics of the deposited material to a minimum. In order to satisfy these two conditions, during the deposition of the heterogeneous material (heterojunction), the properties of the surface (interface) of the coated material, must be prominently highlighted. Hence, we propose a simple interface treatment technique using amorphous-carbon (a-C), which is advantageous in terms of economics, speed, accuracy, and reliability, as described above. This technique can be used to realise powerful synthesis, deposition, and coating.

Result and Discussion

Morphologies and microstructures of a-C. The conditions and preparation of a-C as a coating are described in the methods section and Fig. 1. Supplementary information (SI), Fig. S1 shows SEM images of cases where a-C is applied in the form of a thin film and a core-shell to an alumina substrate and SnO₂ nanowires (NWs), respectively. In the case of the alumina substrate, it was observed that nanoparticles aggregated when a-C was deposited on the alumina surface. These a-C particles could be determined by adjusting the synthesis temperature or process time (the corresponding images are not shown). Then, the a-C particles can be considered as heterogeneous nucleation mechanisms rather than homogeneous nucleation mechanisms based on the grain boundaries of existing alumina substrates. In the case of the SnO₂ NWs, the results show that this synthesis technique was applied successfully. SI, Figs. S1g,h indicate that an a-C structure can be formed in spaces between SnO₂ NWs as well as on the surface of SnO₂ NWs. The crystallisation characteristics of a-C microstructures that can be simultaneously applied to thin films and NWs of SnO₂ (Fig. 2a) were confirmed by transmission electron microscopy (TEM; Fig. 2d,g,k,l), high-resolution TEM (HRTEM; Fig. 2b,e), selected-area electron diffraction (SAED; Fig. 2c,f) patterns, mapping (Figs. 2h–j), and point energy dispersive X-ray spectroscopy (EDX, Fig. 2m–o). HRTEM and SAED patterns were observed for each part (SnO₂ core and a-C shell) of the SnO₂ NWs to investigate the crystallinity of SnO₂ NWs covered by a-C. It was found that single crystals of SnO₂ were represented by spotty patterns and a-C was represented by hazy circles. In particular, as seen in Fig. 2f, the presence of blurred circles in the spotty pattern of SnO₂ implies the possibility of the transfer of properties different from those of the existing materials without significantly affecting the original characteristics of the existing materials. The mapping results confirm that the a-C (Fig. 2h) uniformly covers the preformed SnO₂ NWs (Fig. 2i,j). With regard to the distribution of carbon, the concentration at the surface of the SnO₂ NWs is the greatest, which indicates the nature of the surface of the SnO₂ NWs (or the nature of the interface between SnO₂ and a-C) (Fig. 2h). The composition and properties of carbon were reaffirmed using point EDX (Fig. 2m–o). That is, the deposition layer, which can cover the surface of the material easily, similar to a fluid, is almost entirely carbon (Fig. 2m,o), most of which is present at the interface of the existing materials. This means that there is hardly any interdiffusion of atoms in the existing heterogeneous junctions. In summary, only the energy characteristics of the SnO₂ interface at which all reactions occur are changed while the inherent characteristics of the SnO₂ are maintained.

Properties of SnO₂/a-C core-shell interface. Figure 3 presents evidence index results that show the coating properties of the SnO₂ cores and a-C shell structures. The XRD results (Fig. 3a) indicate that a-C does not exhibit its own crystalline properties and can affect only by bonding with other materials (SnO₂). The XRD patterns for the deposition on the existing substrate (pink) and the coating on the SnO₂ NWs (red) do not exhibit their own unique peaks. This tendency is also prominent in the results of the Raman (Fig. 3b) and PL (Fig. 3c) measurements. However, even if its own characteristics are not apparent, the effects of a-C cannot be ignored, as the existing peaks vary in intensity. This difference can clearly be observed in the XPS results of the a-C binding energies in the a-C thin film and SnO₂/a-C shown in Fig. 3d,e, respectively. The binding originally exhibited by a-C is dominated by sp³ binding rather than sp² binding (Fig. 3d). However, when a-C binds with SnO₂, sp² binding becomes more significant than sp³ binding, and the remaining C-O-C binding peak is significantly reduced (Fig. 3e). In other words, a-C does not have any effect on its own, but its combination with other materials can result in the creation of new properties at the interface.

Energy exchange between materials. As described above, although the physical and chemical properties of base materials can be changed or highlighted via deposition of a-C, there is still insufficient evidence to assert this conclusion. Therefore, ultraviolet photoelectron spectroscopy (UPS), which can be used to infer the mutual energy band by combining with the a-C, is used to clarify the differences in the valence band maximum and the work function of the preformed SnO₂. Figure 4a presents the energy bands of a-C, SnO₂, and SnO₂/a-C. From the results of the incident energy and Fig. 4d,f,h, the work functions of a-C, SnO₂, and SnO₂/a-C are 0.5 eV, 4.4 eV, and 4.7, respectively, as shown in Fig. 4b. The difference between 4.4 eV and 4.7 eV can be assumed to be related to energy exchange before and after the deposition of a-C on SnO₂. The changes in the valence band maximum of a-C, SnO₂, and SnO₂/a-C were 13 eV (12.5 eV V 10.5 eV, Figs. 4b,c, and 5a), 8.15 eV (3.75 eV V 34.4 eV,

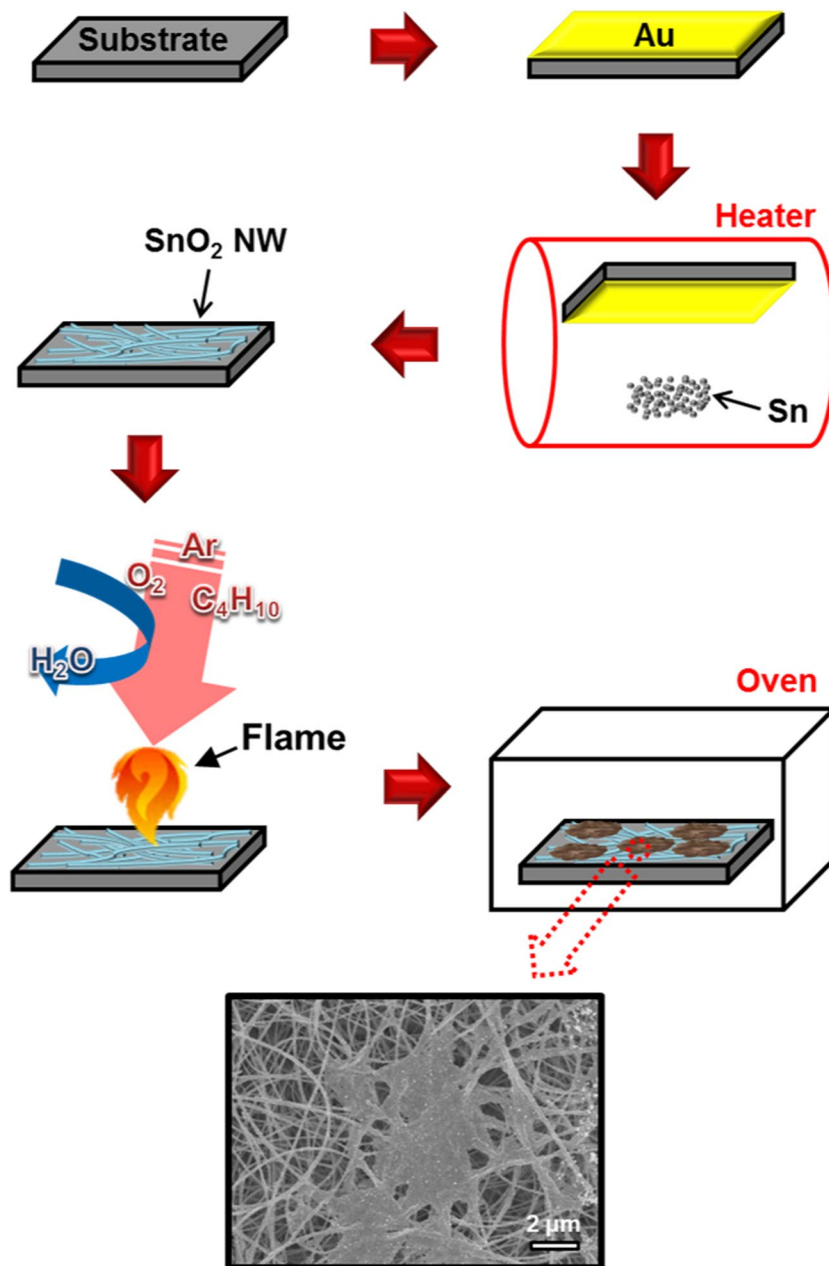


Figure 1. Synthesis of SnO₂/a-C core-shell structure. SnO₂ was formed via thermal evaporation of Sn powder using a Au catalyst on an alumina substrate, and the a-C thin film was obtained by applying a spark to water, which was drained and deposited on the SnO₂ NWs.

Figs. 4b,e and 5a), and 5.2 eV (0.5 eV V04.7 eV, Figs. 4b,g and 5a), respectively, on the basis of the vacuum level. This means that there is some energy interchange between SnO₂ and a-C, which is a result of a completely new property based on the combination of SnO₂ and a-C. To understand why this difference occurs and the exact role of a-C in it, let us consider all the possible predictions presented above by applying them directly to applications under different conditions with sensitive surface gas sensing. We must also understand how a-C works in combination with the existing materials. Therefore, in order to investigate the above predictions, we studied gas-sensing applications under different conditions because it is most sensitive to the surface. Based on this, the mechanism through which a-C combines with the existing material was deduced.

Mechanism behind change in SnO₂/a-C interface and gas sensing. Based on the UPS results (Fig. 4), the energy states for each material were deduced, as shown in Fig. 5a. The core-shell structure of SnO₂/a-C had a valence band maximum of 5.2 eV and a Fermi level of 4.7 eV from the vacuum level. This energy structure exhibits superior gas-sensing characteristics with regard to process temperatures, responses, response times, and recovery times, compared to conventional gas sensing with bare SnO₂ NWs^{33–35}. This can be attributed to the a-C mechanism, which is optimised for the most prominent gas sensing, where the interfacial characteristics

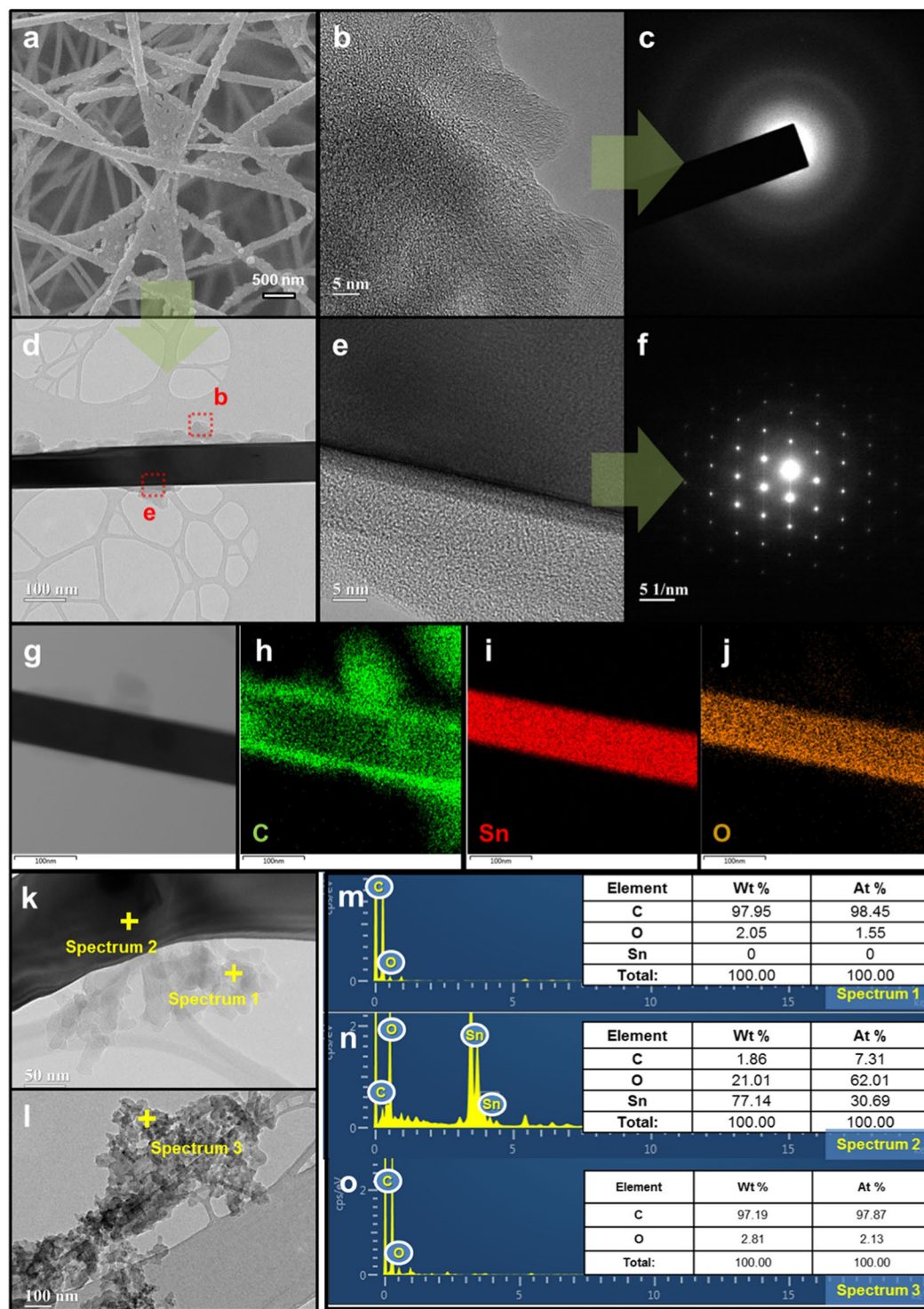


Figure 2. Morphology, crystallinity, and elemental composition of SnO₂/a-C. (a) SEM image of SnO₂ coated with a-C; (b) HRTEM image of a-C as the coating layer; (c) SAED pattern of a-C; (d) single SnO₂/a-C core-shell structure; (e) HRTEM image of SnO₂/a-C interface; (f) SAED pattern of mixture of monocrystalline SnO₂ and a-C; (g) TEM image of SnO₂/a-C before mapping; distribution of (h) C, (i) Sn, and (j) O in SnO₂/a-C; (k) TEM image of SnO₂/a-C interface; (l) TEM image of a-C; point EDX results of (m) a-C shell, (n) SnO₂ core, and (o) a-C.

of the sample are more important than other factors during the gas measurement. In general, gas sensors are driven by activated carriers at the sample surface. However, the deposition of a-C on the SnO₂ surface results in a lower energy barrier that can respond to gas sensing on the surface. Therefore, even if the bare SnO₂ NWs do not

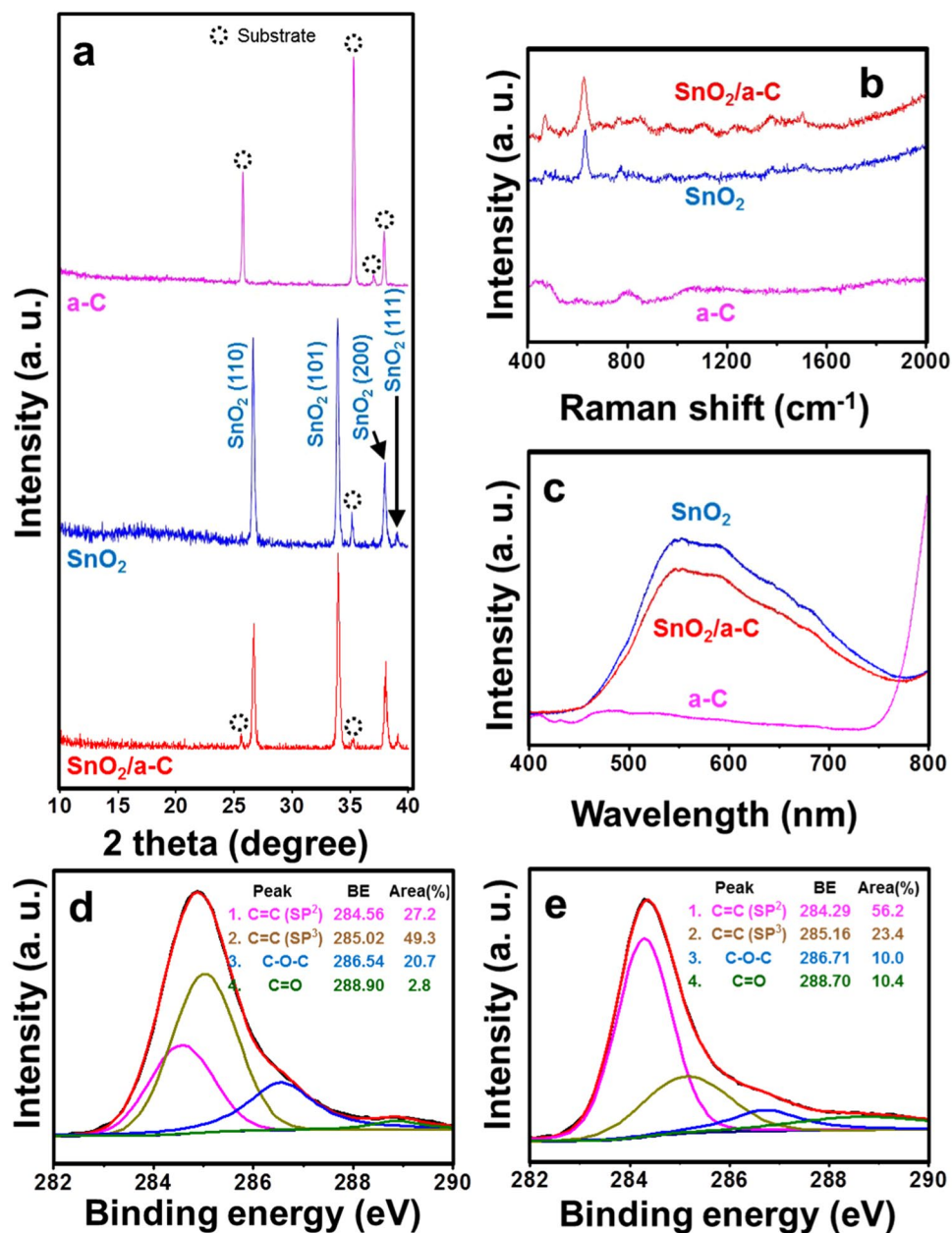


Figure 3. Analysis of chemical bonding of a-C, SnO₂, and SnO₂/a-C. (a) XRD results, (b) Raman spectra, and (c) PL of each sample; XPS results after deposition of a-C on (d) alumina substrate and (e) SnO₂ NWs.

exhibit gas-sensing characteristics due to the small number of activated carriers at room temperature, the NO₂ gas-sensing ability can be improved six-fold by combining a-C with SnO₂ (Fig. 5b). This is proof of the interfacial characteristics, where the energy equilibrium is changed due to the heterojunction. This tendency can further improve the sensing characteristics at 100 °C, 200 °C, and 300 °C, where there is a high carrier concentration at the interface. However, there are limits to increasing the interfacial reactivity to NO₂ gas unlike in the case of conventional SnO₂ surfaces (SI, Fig. S2a). In other words, the gas characteristics are not necessarily improved even with constantly high temperatures. As seen in Fig. 5b, if the temperature reaches a critical point between 200 °C and 300 °C, the a-C no longer increases the surface properties of SnO₂, but can have other mechanisms. Therefore, the interfacial change according to the temperature dependence of a-C needs to be studied more accurately in the future. However, there is a difference between the SnO₂/a-C characteristics that must be considered. In the analysis method of Fig. 3, the incident energy from the analytical tool passes through the interface between the a-C and the SnO₂, whereas the gas-sensing reaction mechanism shown in Fig. 5b almost stops at the SnO₂ interface. In other words, the role of a-C, which results in changes or improvements in the properties of the existing SnO₂ materials, is the same, but the gas-sensing reaction mechanism is the most sensitive to surface reactions compared to other analytical methods. SI, Fig. S2b–e show the NO₂ gas-sensing response and the response and recovery times at various temperatures for the SnO₂/a-C sample. Compared with those of bare SnO₂, the surface response

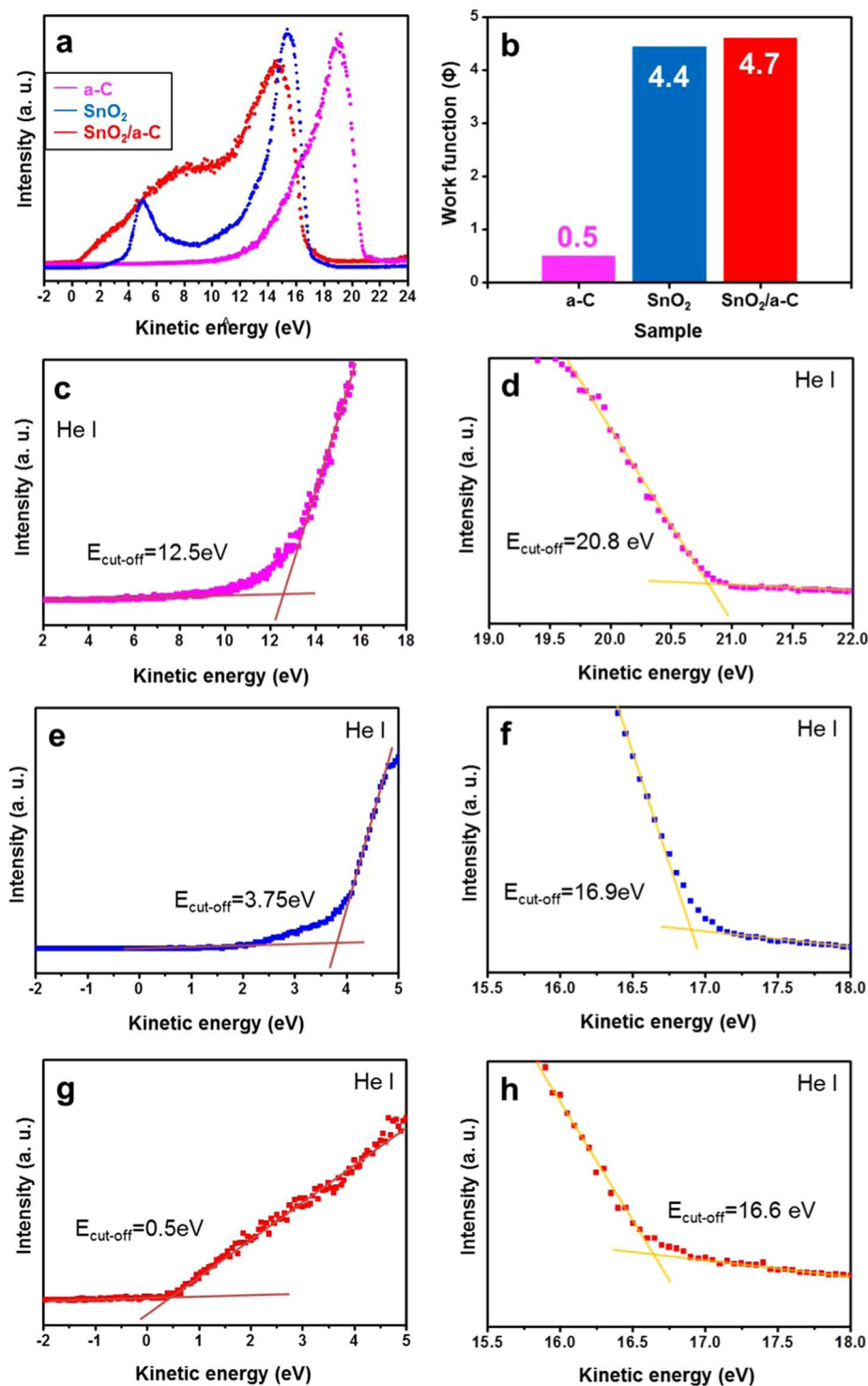


Figure 4. UPS results of a-C, SnO₂, and SnO₂/a-C. (a) UPS of a-C, crystalline SnO₂, and SnO₂/a-C core-shell; (b) work functions of a-C, SnO₂, and SnO₂/a-C; (c) valence band maximum of 12.5 eV and (d) energy_(cut-off) of 20.8 eV for work function of 0.5 eV in a-C (i.e., $21.2 \text{ eV}_{(\text{incident energy})} - 0.1 \text{ eV}_{(\text{correction value})}$); (e) valence band maximum of 3.75 eV and (f) energy_(cut-off) of 16.9 eV for work function of 4.4 eV in monocrystalline SnO₂ (i.e., $21.2 \text{ eV}_{(\text{incident energy})} - 16.9 \text{ eV} + 0.1 \text{ eV}_{(\text{correction value})}$).

sensitivities of SnO₂/a-C are far superior, as expected, demonstrating excellent response time and recovery time in all temperature ranges. These representative gas-sensing indices before and after the a-C process is applied are presented in Supplementary Table 1.

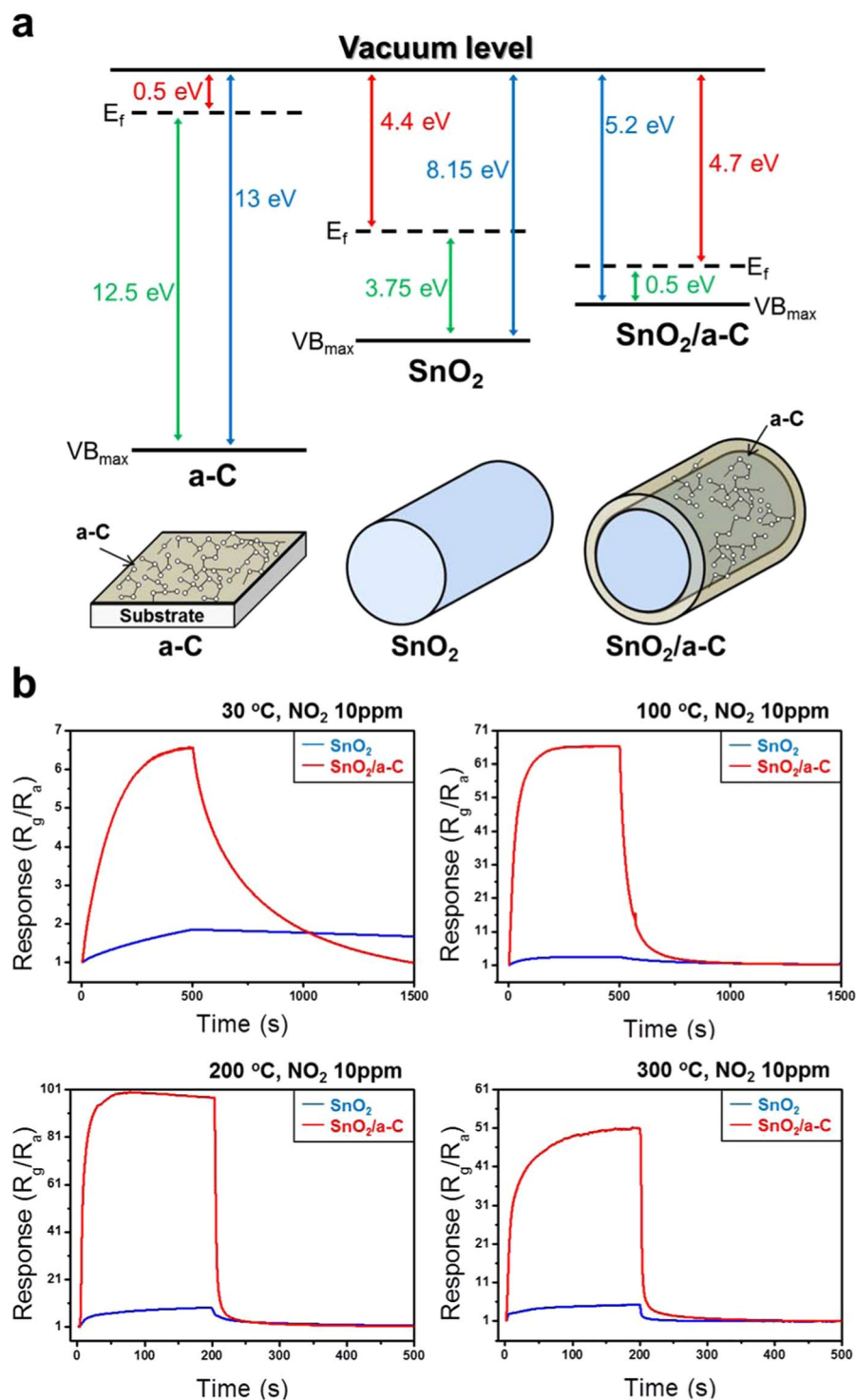


Figure 5. Comparison of energy states and 10 ppm NO₂ gas-sensing performance for a-C, SnO₂, SnO₂/a-C. (a) Energy relationship between Fermi level, valence band maximum, and work function; (b) response at 30 °C, 100 °C, 200 °C, and 300 °C for SnO₂ and SnO₂/a-C core-shell structures.

As seen, instead of a crystalline shell, a-C can be deposited on a material to enhance its surface properties or to convert it into a new material. This can result in new functions in a short time, and it is expected to be widely used for industrial applications in the future because of its superior convenience and accessibility compared to other processes.

Discussion

A coating method using a-C that can be easily and variously applied is suggested as a method of deposition on a base material. This method can improve the surface reactivity of existing materials while showing little of their physicochemical properties unlike existing heterogeneous junctions. Especially in the case of a-C, regardless of the surface state of the material, it is strongly adsorbed on the preformed material by controlling the process temperature or the process time. Only surface (or interface) characteristics of the existing material can be significantly enhanced. These surface sensitivities were measured using SEM, TEM, XRD, Raman, PL, XPS, and gas-sensing mechanisms. In particular, the NO₂ gas-sensing ability of SnO₂/a-C was almost six times better than that of bare-SnO₂ even at room temperature. Therefore, if the a-C process parameters are controlled and the changes in each process condition are easily grasped at a glance, this advanced engineering technology can be applied to various industrial fields. This approach is also significant because it is a breakthrough that can be studied, without regard to materials and environment and without the need for expensive vacuum technology.

Methods

As shown in Fig. 1, a home-made pyrotechnic device with a temperature range of 500–1200 °C was prepared for depositing a-C on a material. a-C was deposited onto thin films of an alumina substrate and as a shell coating of core SnO₂ NWs. For the thin film, a spark was applied directly on the water, and a-C deposited on the water was drained and deposited on the alumina substrate. For the coating of the SnO₂ NWs, the alumina substrate on which the SnO₂ NWs were grown was used instead of a bare alumina substrate, while maintaining process methods such as thin film formation methods. The SnO₂ NWs were produced using a thermal evaporation method with a Au catalyst at 900 °C for 1 h using 97% Ar and 3% O₂ gases.

The morphologies of the SnO₂/a-C core-shell structures were analysed using SEM (Hitachi S-4200) and TEM (200 kV, JEOL JEM-2010, Japan). HRTEM and SAED equipped with TEM and XRD (Philips X-pert MRD X-ray diffractometer) were used for microstructure analysis. The SnO₂ and SnO₂/a-C structures were analysed qualitatively and quantitatively via mapping and EDX with a TEM, and the chemical bonds on the surface were compared using Raman spectroscopy (LabRAM HR800, Jobin Yvon, France), PL (LabRAM HR800, Jobin Yvon, France), and XPS (K-Alpha plus, Thermo Fisher Scientific Inc., USA) analyses. In addition, the energy relationships of each component, such as the valence band maximum, work function, and Fermi level, were determined using UPS (Theta probe base system, Thermo Fisher Scientific Inc., USA). Gas sensing was performed with NO₂, an oxidising gas. A semiconductor-based method in which the resistance changes depending on the degree of adsorption of gas was used for the gas-sensing experiment. The concentration of NO₂ was fixed at 10 ppm, and the temperature range for sensing was from room temperature to 300 °C with 100 °C intervals.

Data availability

All the data are available from the corresponding author on reasonable request.

Received: 17 November 2019; Accepted: 29 January 2020;

Published online: 05 March 2020

References

- Rasmussen, F. E., Ravnkilde, J. T., Tang, P. T., Hansen, O. & Bouwstra, S. Electroplating and characterization of cobalt–nickel–iron and nickel–iron for magnetic microsystems applications. *Sens. Actuators B-Chem.* **92**, 242–248 (2001).
- Liu, J. B. *et al.* Synthesis of bimetallic nanoshells by an improved electroless plating method. *Langmuir* **21**, 1683–1686 (2005).
- Yi, L., Zhiyuan, L., Shuoshuo, C., Xing, H. & Xinhua, H. Novel AAO films and hollow nanostructures fabricated by ultra-high voltage hard anodization. *Chem. Commun.* **46**, 309–311 (2010).
- Yang, D. *et al.* Chemical analysis of graphene oxide films after heat and chemical treatments by X-ray photoelectron and Micro-Raman spectroscopy. *Carbon* **47**, 145–152 (2009).
- Fridman, A. *Plasma chemistry* (Cambridge, 2008).
- Kablitz, C. D. *Dry coating: a characterization and optimization of an innovative coating technology* (Cuvillier Verlag, 2007).
- Wang, L., Meng, C., Liu, C. & Wang, L. Glass-ceramic protective coating for titanium alloys. *J. Am. Ceram. Soc.* **85**, 2867–2869 (2002).
- Zhang, Y., Ge, D. & Yang, S. Spray-coating of superhydrophobic aluminum alloys with enhanced mechanical robustness. *J. Colloid. Interf. Sci.* **423**, 101–107 (2014).
- Chen, S. *et al.* Oxidation resistance of graphene-coated Cu and Cu/Ni alloy. *ACS Nano* **5**, 1321–1327 (2011).
- Streitberger, H. J. & Dössel, K. F. *Automotive paints and coatings* (Wiley-VCH, 2008).
- Noordin, M. Y., Venkaesh, V. C., Sharif, S., Elting, S. & Abdllah, A. Application of response surface methodology in describing the performance of coated carbide tools when turning AISI 1045 steel. *J. Mater. Process. Tech.* **145**, 46–58 (2004).
- Haron, C. G. C., Ginting, A. & Arshad, H. Performance of alloyed uncoated and CVD-coated carbide tools in dry milling of titanium alloy Ti-6242S. *J. Mater. Process. Tech.* **185**, 77–82 (2007).
- Hamasaiid, A. *et al.* Effect of mold coating materials and thickness on heat transfer in permanent mold casting of aluminum alloys. *Metall. Mater. Trans. A* **38**, 1303–1316 (2007).
- Wang, J. *et al.* Epitaxial BiFeO₃ multiferroic thin film heterostructures. *Science* **299**, 1719–1722 (2003).
- Lauhon, L. J., Gudiksen, M. S., Wang, D. & Lieber, C. M. Epitaxial core–shell and core–multishell nanowire heterostructures. *Nature* **420**, 57–61 (2002).
- Chen, C.-W. *et al.* Efficient and uniform planar-type perovskite solar cells by simple sequential vacuum deposition. *Adv. Mater.* **26**, 6647–6652 (2014).
- Mattox, D. M. *The foundation of vacuum coating technology* (Springer, 2003).
- Wang, Z. -S., Yanagida, M., Sayama, K. & Sugihara, H. Electronic-insulating coating of CaCO₃ on TiO₂ electrode in dye-sensitized solar cells: improvement of electron lifetime and efficiency. *Chem. Mater.* **18**, 2912–2916 (2006).
- Pénard, A.-L., Gacoin, T. & Boilot, J.-P. Functionalized sol–gel coatings for optical applications. *Acc. Chem. Res.* **40**, 895–902 (2007).
- Wen, C. *Surface coating and modification of metallic biomaterials* (Woodhead Publishing, 2015).
- Bhushan, B. *Biomimetics: bioinspired hierarchical-structured surfaces for green science and technology* (Springer, 2016).
- Sanchez, C., Arribart, H. & Guille, M. M. G. Biomimetism and bioinspiration as tools for the design of innovative materials and systems. *Nat. Mater.* **4**, 277–288 (2005).
- Chauhan, B. P. S. *Hybrid Nanomaterials: Synthesis, Characterization, and Applications* (Wiley, 2011).

24. Sanchez, C., Belleville, P., Popall, M. & Nicole, L. Applications of advanced hybrid organic–inorganic nanomaterials: from laboratory to market. *Chem. Soc. Rev.* **40**, 696–753 (2011).
25. Poedt, P. *et al.* High-speed spatial atomic-layer deposition of aluminum oxide layers for solar cell passivation. *Adv. Mater.* **22**, 3564–3567 (2010).
26. Kaelin, M., Rudmann, D. & Tiwari, A. N. Low cost processing of CIGS thin film solar cells. *Sol. Energy* **77**, 749–756 (2004).
27. Hata, K. *et al.* Water-assisted highly efficient synthesis of impurity-free single-walled carbon nanotubes. *Science* **306**, 1362–1364 (2004).
28. Vossen, J. L. & Kern, W. *Thin film processes II* (Academic Press, 2012).
29. Razeghi, M. *The MOCVD Challenge: A survey of GaInAsP-InP and GaInAsP-GaAs for photonic and electronic device applications* (CRC Press, 2010).
30. Pinna, N. & Knez, M. *Atomic layer deposition of nanostructured materials* (Wiley-VCH, 2012).
31. Behrisch, R. & Eckstein, W. *Sputtering by particle bombardment: experiments and computer calculations from threshold to MeV energies* (Springer, 2007).
32. Holzapfel, C., Rubie, D. C., Frost, D. J. & Langenhorst, F. Fe-Mg interdiffusion in (Mg, Fe) SiO₃ perovskite and lower mantle reequilibration. *Science* **309**, 1707–1710 (2005).
33. Sharma, A., Tomar, M. & Gupta, V. SnO₂ thin film sensor with enhanced response for NO₂ gas at lower temperatures. *Sens. Actuators B-Chem.* **156**, 743–752 (2011).
34. Shaalan, N. M., Yamazaki, T. & Kikuta, T. Influence of morphology and structure geometry on NO₂ gas-sensing characteristics of SnO₂ nanostructures synthesized via a thermal evaporation method. *Sens. Actuators B-Chem.* **153**, 11–16 (2011).
35. Kaur, J., Roy, S. C. & Bhatnagar, M. C. Highly sensitive SnO₂ thin film NO₂ gas sensor operating at low temperature. *Sens. Actuators B-Chem.* **123**, 1090–1095 (2007).

Acknowledgements

This research was supported by Basic Science Research Program through the National Research Foundation of Korea (NRF) funded by the Ministry of Education (NRF-2017R1A6A3A11030900 and 2019R1A6A1A11055660 and 2016R1A6A1A03013422). We are grateful to Jiye Kim, Mun Young Koh, Baro Jin, Ha Jin Na, and Koh Eun Na for their cordiality and hospitality during the course of this research.

Author contributions

M.S.C. and H.G.N. developed the concept and H.W.K. and C.J. wrote the manuscript. M.S.C., H.G.N. and J.H.B. fabricated the samples and performed the measurements. S.-W.C., S.S.K. and K.H.L. provided theoretical basis. All authors contributed to interpretation of the fundamental theories, discussed the issues, and exchanged views on the manuscript.

Competing interests

The authors declare no competing interests.

Additional information

Supplementary information is available for this paper at <https://doi.org/10.1038/s41598-020-61141-9>.

Correspondence and requests for materials should be addressed to H.W.K. or C.J.

Reprints and permissions information is available at www.nature.com/reprints.

Publisher's note Springer Nature remains neutral with regard to jurisdictional claims in published maps and institutional affiliations.



Open Access This article is licensed under a Creative Commons Attribution 4.0 International License, which permits use, sharing, adaptation, distribution and reproduction in any medium or format, as long as you give appropriate credit to the original author(s) and the source, provide a link to the Creative Commons license, and indicate if changes were made. The images or other third party material in this article are included in the article's Creative Commons license, unless indicated otherwise in a credit line to the material. If material is not included in the article's Creative Commons license and your intended use is not permitted by statutory regulation or exceeds the permitted use, you will need to obtain permission directly from the copyright holder. To view a copy of this license, visit <http://creativecommons.org/licenses/by/4.0/>.

© The Author(s) 2020